RESEARCH

Graphene-Loaded Surface Plasmon Polariton (SPP) Waveguide Surrounded by Uniaxial Chiral (UAC) and Plasma Layers

Mutasem Z. Bani-Fwaz[1] · R. Bousbih[2] · Raad A. Khamis[3] · Mohamed S. Soliman[4] · Majid S. Jabir[5] · Hasan Majdi[6] · Mohamed Shaban[7] · Essam Elsayed Assem[7] · Sameerah I. Al-Saeedi[8] · N. M. A. Hadia[9] · Laiba[10]

Abstract

In this manuscript, we have developed a model for a graphene-loaded surface plasmon polariton waveguide surrounded by uniaxial chiral and plasma layers. Electromagnetic wave theory is utilized to solve numerical problems. Graphene conductivity is modeled physically using the Kubo formula, described in the "Methodology" section. The characteristic equation is obtained by applying boundary conditions at $x = 0$. Based on numerical calculations, we examine the impact of chemical potential, number of graphene layers, plasma frequency, collisional frequency, and chirality on normalized propagation constants. Furthermore, the cutoff frequency for two different cases of the uniaxial chiral medium used for the different values of graphene and plasma parameters is revealed. The numerical results reflect that the presented study can be used to fabricate modulator plasmonic devices ranging from sensing and imaging to communication in the terahertz frequency regime.

Keywords Plasmon · Uniaxial chiral · Graphene · Plasma · Characteristic equation · Waveguide

Introduction

The rapid advancement of semiconductors and integrated circuits in microelectronics offers a solid foundation for many applications, most notably in communication and information processing. Despite this, further innovation in the field of information transmission is always constrained by the efficiency of electronic components because electrons are inherently capable of carrying less data. Photonics may offer an alternative solution to this problem, as photons can carry more information and travel faster. Most recently, it has been demonstrated that the trade-off between capacity and size can be minimized quite effectively by making use of surface plasmon polaritons. The fundamental concept here is that electromagnetic waves, which are normally propagated within a dielectric waveguide, can propagate along the metal surface through surface plasmon-polariton (SPP) phenomena [1–6]. The subwavelength mode confinement of the surface plasmon polariton (SPP) mode makes plasmonic waveguides more flexible in size than dielectric waveguides. In this context, SPP has the potential to be a crucial technology for next-generation nanophotonic devices [7]. The major disadvantage of current plasmonic waveguides is that they have very serious propagation loss

particularly if the mode confinement scales down to the subwavelength range [8]. In general, all SPP modes have this fundamental drawback: stronger confinement causes the field to move closer to the metal, which leads to serious energy losses, resulting in a shorter propagation length [9]. To accomplish tight mode confinement through plasmonic waveguides with relatively low propagation losses, novel plasmonic waveguide structures are needed in the optic community. In the optical sector, there is an increasing demand for plasmonic materials to overcome these challenges [10].

Recently, graphene revolutionized the optical sector for developing photonic devices due to its extraordinary optical and electrical properties [11–16]. The zero-band gap structure of graphene has made it a promising alternative candidate for overcoming the deficiencies of metallic-based optoelectronic devices and an ideal candidate for developing broadband saturable absorbers. It has also been reported that graphene's electron mobility reaches up to 200,000 cm^2/Vs, which could enable the design of high-performance modulators and photodetectors. Furthermore, graphene-based photonic devices have a remarkable potential for biochemical sensing applications due to their large surface area and high adsorption capacity. By tailoring the carrier density in graphene, the adsorbed chemical molecules can also modify the optical traits of photonic devices [17, 18].

Extended author information available on the last page of the article

Chiral material that exhibits nondirectional chirality is known as a UAC material [19]. Interestingly, the process of manufacturing uniaxial chiral mediums is very convenient and easy to do [20]. As a standard procedure, UAC materials are produced by the immersion of small chiral items (such as wire spirals) in an anisotropic medium [21]. Vapor deposition processes can be used to produce such a medium in a very straightforward manner [22]. UAC mediums are anticipated many fascinating features by virtue of their chirality coupled with anisotropy. In this manuscript, the numerical analysis of SPPs at UAC-metal-UAC in the visible spectrum is analyzed. Three cases of UAC medium are studied to demonstrate the influence of chirality and core width on effective mode index as the function of wave frequency.

Plasma is the highly ionized state of gas comprising electrons, ions, and neutral particles. Optic researchers have taken a keen interest in studying electromagnetic surface wave traits in a plasma medium. Numerous fields have taken advantage of the unexceptional response of electromagnetic waves in a plasma medium, including biochemical sensing, spectroscopy, light-trapping devices, optoelectronic devices, and communications. In the plasma medium, EM surface waves are affected by numerous factors such as collision frequency, plasma frequency, and operating frequency. Electromagnetic waves in plasma are affected by these properties, which determine their absorption, reflection, and transmission attributes [23–26]. Compared to conventional dielectrics, plasma shows distinct characteristics. Among them is the plasma's permittivity which can be controlled by altering the number density of electrons. Plasma also offers the advantage of reducing absorption losses in nanophotonic devices. The efficiency of nanophotonic devices is limited by absorption problems in traditional dielectrics, such as silicon and gallium arsenide. This loss can be minimalized by introducing plasma, since plasma acts as a low-loss medium, resulting in a lower absorption rate and a higher light transmission rate [27]. Thus, the literature review motivated us to conduct the study of graphene-loaded SPP waveguides surrounded by uniaxial chiral and plasma layers.

Methodology

A planar graphene-loaded waveguide structure surrounded by UAC and plasma layer is shown in Fig. 1. Here, we present the characteristic equation for the proposed waveguide structure. Let us consider the SPPs propagating along the z-axis while attenuating along the x-axis.

The EM waves in the UAC medium are described by the following constitutive relations.
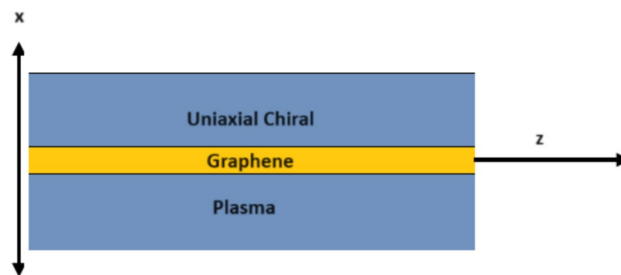

Fig. 1 Schematic configuration of graphene-loaded SPP waveguide surrounded plasma uniaxial chiral and plasma layer

$$\boldsymbol{D} = \left[\varepsilon_t \bar{\bar{I}}_t + \varepsilon_z \hat{e}_z \hat{e}_z\right].\mathbf{E} - j\xi_c \sqrt{\mu_0 \varepsilon_0}\hat{e}_z \hat{e}_z.\mathbf{H}$$
$$\boldsymbol{B} = \left[\mu_t \bar{\bar{I}}_t + \mu_z \hat{e}_z \hat{e}_z\right].\mathbf{H} - j\xi_c \sqrt{\mu_0 \varepsilon_0}\hat{e}_z \hat{e}_z.\mathbf{E} \tag{1}$$

Here, ξ represents the chirality parameter, and ε_0 and μ_0 describe the permittivity and permeability of free space, respectively.

$$E_z = K_1 e^{-q_1 x} + K_2 e^{-q_2 x} \tag{2}$$

$$H_z = \frac{j\alpha_{1,2}}{\eta_t}(K_1 e^{-q_1 x} + K_2 e^{-q_2 x}) \tag{3}$$

Here, q_1 and q_2 are the wavenumbers of the UAC medium. Other EM field components can be derived from [27, 28]:

$$E_t = \left(-\frac{j\beta\nabla_t}{q_1^2} - \frac{\nabla_t k_t \alpha_1}{q_1^2}\hat{e}_z\right)K_1 e^{-q_1 x} + \left(-\frac{j\beta\nabla_t}{q_2^2} - \frac{\nabla_t k_t \alpha_1}{q_2^2}\hat{e}_z\right)K_2 e^{-q_2 x} \tag{4}$$

$$q_{1,2}^2 = \frac{\lambda^2}{2}\left[\frac{\mu_z}{\mu_t} + \frac{\varepsilon_z}{\varepsilon_t} + \sqrt{\left(\frac{\mu_z}{\mu_t} - \frac{\varepsilon_z}{\varepsilon_t}\right)^2 + \frac{4\xi^2 \mu_z \varepsilon_z}{\mu_t \varepsilon_t}}\right] \tag{5}$$

Here,

$$\lambda^2 = \beta^2 - \omega^2 \mu_t \varepsilon_t \tag{6}$$

$$\alpha_1 = \left(\frac{q_1^2}{\lambda^2} - \frac{\varepsilon_z}{\varepsilon_t}\right)\frac{\sqrt{\mu_t \varepsilon_t}}{\xi\sqrt{\mu_z \varepsilon_z}} \tag{7}$$

$$\alpha_2 = \left(\frac{q_2^2}{\lambda^2} - \frac{\varepsilon_z}{\varepsilon_t}\right)\frac{\sqrt{\mu_t \varepsilon_t}}{\xi\sqrt{\mu_z \varepsilon_z}} \tag{8}$$

$$\eta_t = \sqrt{\varepsilon_t / \mu_t} \tag{9}$$

According to Kubo formula, the graphene conductivity is given as follows:

$$\sigma\left(\mu_c, \tau, \mathrm{T}\right) = \frac{je^2\left(\omega - j\tau^{-1}\right)}{\pi h^2} \times \left[\frac{1}{\left(\omega - j\tau^{-1}\right)^2} \int_0^\infty \times \xi_n \left(\frac{\sigma f_d\left(\xi_n, \mu_c, T\right)}{\sigma \xi_n} - \frac{\sigma f_d\left(-\xi_n, \mu_c, T\right)}{\sigma \xi}\right) d\xi_n - \int_0^\infty \times \frac{f_d\left(-\xi_n, \mu_c, T\right) - f_d\left(\xi_n, \mu_c, T\right)}{\left(\omega - j\tau^{-1}\right)^2 - 4(\xi_n/\hbar)^2} d\xi_n\right]$$

where $j, \xi_n, \hbar f_d, \mu_c, \tau, \mathrm{T}, e$, and ω represent the imaginary unit, energy, reduced Plank's constant Fermi–Dirac distribution, chemical potential, relaxation time, temperature, charge on electron, and operating frequency, respectively.

The EM fields for the plasma medium are given below:

$$E_z = K_3 e^{k_p x} \tag{11}$$

$$H_z = K_4 e^{k_p x} \tag{12}$$

$$E_y = -\frac{j\omega\mu_0 K_4 e^{k_p x}}{k_p} \tag{13}$$

$$H_y = -\frac{j\omega\varepsilon_p K_3 e^{k_p x}}{k_p} \tag{14}$$

Here, k_p is the wavenumber in a plasma medium $k_p = \sqrt{\beta^2 - \omega^2\varepsilon_p\mu_0}$ [29] and ε_p is the permittivity of isotropic plasma medium $\varepsilon_p = 1 - \frac{\omega_p^2}{\omega^2 + i\omega v}$. ω_p and v represent the plasma frequency and collisional frequency of plasma medium, respectively [30].

$$\hat{x} \times \left[H_1 - H_2\right] = \sigma E \tag{15}$$

$$\hat{x} \times \left[E_1 - E_2\right] = 0 \tag{16}$$

The above boundary conditions are used to obtain the following characteristic equations:

$$\tag{10}$$

$$q_1 q_2(\alpha_1 - \alpha_2)\eta_t\mu_0\omega(k_p\sigma - j\varepsilon_p\omega) + kt^2\alpha_1(\alpha_1 - \alpha_2)\alpha_2 k_p\eta_t$$
$$(-jk_p + \mu_0\sigma\omega) + kt(q_2\alpha_1 - q_1\alpha_2)(k_p^2\eta_t^2\sigma - jk_p$$
$$(\alpha_1\alpha_2\mu_0 + \eta_t^2(\varepsilon_p - \mu_0\sigma^2))\omega + \varepsilon_p\eta_t^2\mu_0\sigma\omega^2) = 0 \tag{17}$$

Results

Here, the characteristics of Eq. (17) are used to elucidate the numerical results of graphene-loaded SPPs surrounded by UAC and plasma layers. Graphene supports the terahertz (THz) frequency regime [6, 12, 31–33]. To investigate the properties of the proposed waveguide structure, two cases of UAC medium are analyzed. The THz spectral region is studied with respect to the normalized propagation constant (NPC) under different graphene and plasma parameters. The NPC is $\mathrm{Re}(\frac{\beta}{k_0})$ where β is the propagation constant and k_0 is the wavenumber in free space.

Case I

In this case, we have set the parameters as follows: $\mu_t = \mu_z = \mu_0$, $\varepsilon_t = -2.3\varepsilon_0$, $\varepsilon_z = -0.1\varepsilon_0$, $\xi = 1.1$, $v = 4 \times 10^6 \mathrm{Hz}$, $\omega_p = 1\mathrm{THz}$, $T = 300K$, $\mu_c = 0.2\mathrm{eV}$, and $\tau = 2\mathrm{ps}$. To investigate the influence of chemical potential, a number of graphene layers on NPC by using Eq. 17 are analyzed in Fig. 2a,b. The operating frequency increases

Fig. 2 Effect of the chemical potential and number of graphene layers on NPC for case I
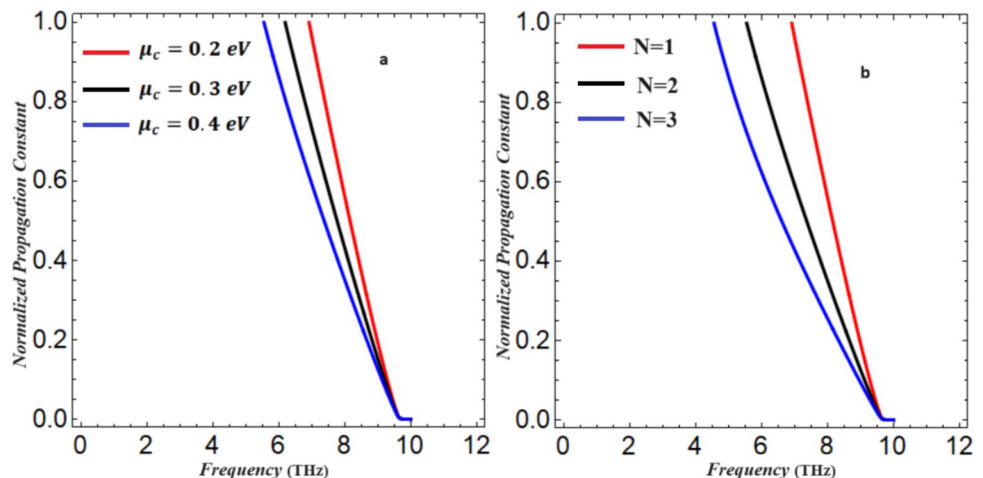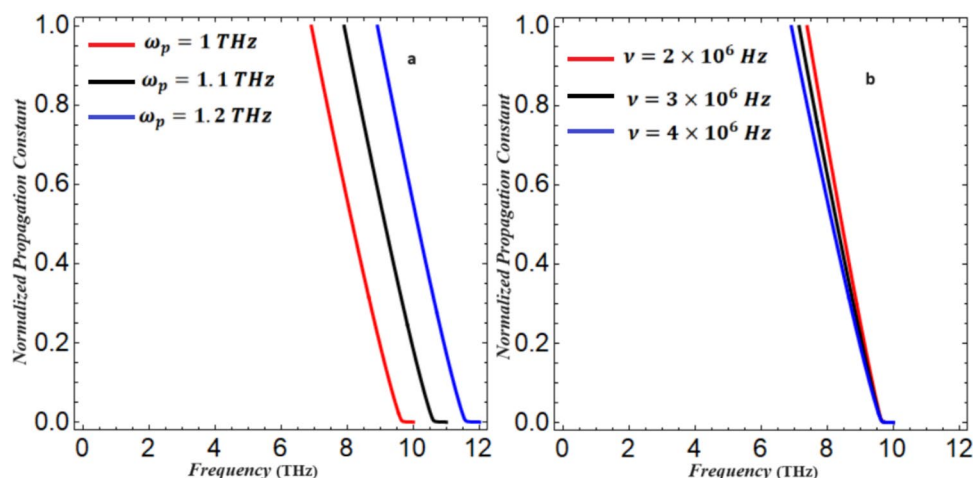
Fig. 3 Effect of the plasma frequency and collisional frequency on NPC for case I

from 0 to 12 THz. In Fig. 2a, chemical potential varies from $\mu_c = 0.2$–$0.4eV$ as shown in red, black, and blue characteristic curves. It can be noted that the variation in NPC significantly varies with chemical potential. Lower values of chemical potential lead to higher NPC as reported in [6, 12, 31–36]. Due to the increasing chemical potential, the energy levels of the graphene lattice become more crowded, resulting in increased scattering and a slower propagation rate. Furthermore, the energy gap between graphene's conduction and valence bands increases with increasing chemical potential. As a result of this energy gap, electrons change their behavior, causing disturbances such as photons and electrons to propagate more slowly. In Fig. 2b, the impact of the number of graphene layers on NPC versus wave frequency is analyzed by using the characteristics of Eq. 17. In a recent study, it was demonstrated that a single layer of graphene absorbs only 2.3% of the incident light [37]. The NPC begins to decrease as the number of graphene layers increases [12, 33, 38, 39]. Due to the stronger interactions between electrons in graphene layers, the scattering of electrons in the graphene layer also becomes stronger, resulting in reduced transmission through the graphene layer. Consequently, a reduction in transmission results in a decrease in wave velocity and a decrease in the NPC. Further analyses of the influence of plasma parameters on the NPC are depicted in Fig. 3a,b. In Fig. 3a, the variation in NPC under the different plasma frequencies is analyzed in the THz wave frequency range. As plasma frequency increases, the cutoff frequency and NPC both increase. A higher plasma frequency leads to an increase in the number of excited plasma particles, thereby producing a stronger coupling with the wave. Thus, there is a greater effective wave velocity, resulting in a larger NPC. In isotropic plasma, plasma frequency plays a vital role in the development of plasmonic-based devices. Furthermore, plasma electrons oscillate at certain frequencies in resonance with the external electromagnetic field, leading to significant enhancements in the scattering properties. Thus,

it is possible to design and fabricate plasmonic devices with diverse functionality by exploiting this resonance phenomenon. Figure 3b depicts the impact of collisional frequency on NPC in a certain wave frequency band. In this context, wave frequency extends from 0 to 12 THz. It can be clearly seen that higher collisional frequency values reflect lower NPC as reported in [27, 30]. When the particles collide with each other at a higher collisional frequency, they can transfer energy to the wave, effectively dampening it. Consequently, this damping effect reduces the amplitude and slows down the propagation of the EM surface wave. Figure 4 depicts the impact of chirality on the NPC. Obviously, lower chirality values lead to higher NPC.
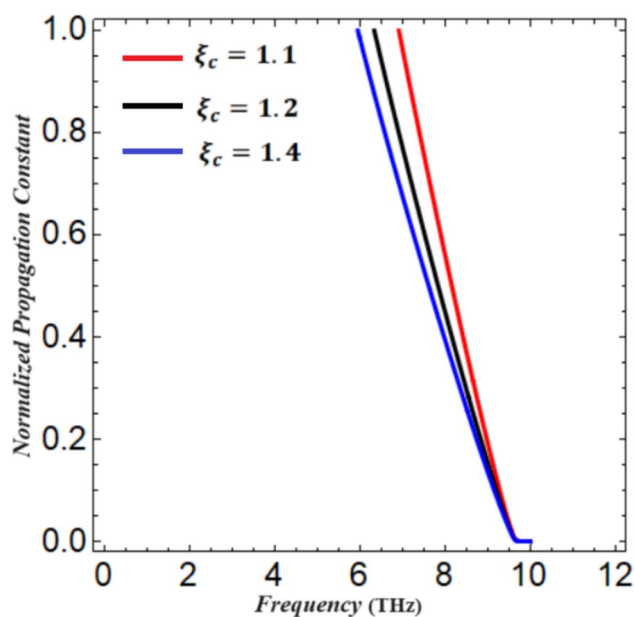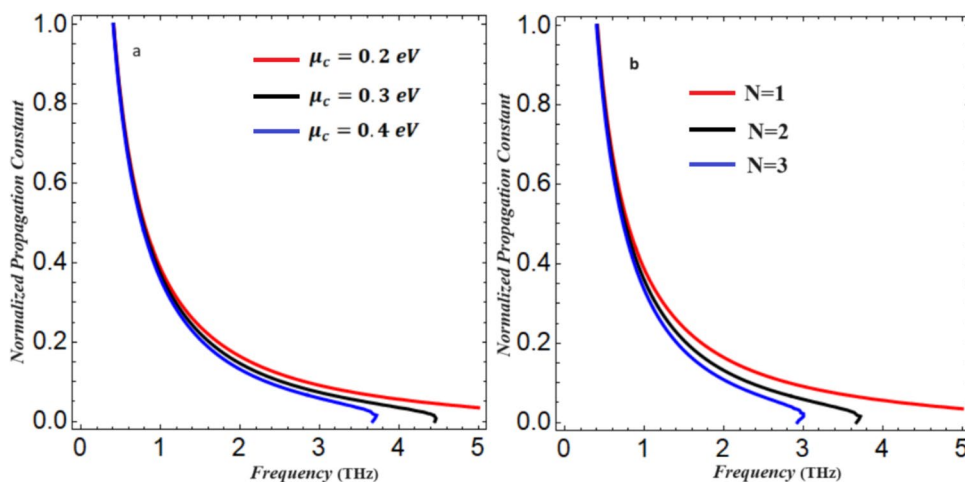

Fig. 4 Effect of the chemical potential and number of graphene layers on NPC for case I

Fig. 5 Influence of the chemical potential and number of graphene layers on NPC for case II

Case II

In this case, we have set the parameters as follows: $\mu_t = \mu_z = \mu_0$, $\varepsilon_t = -2.3\varepsilon_0, \varepsilon_z = 0.1\varepsilon_0, \xi = 1.1, \nu = 4 \times 10^6 \text{Hz}, \omega_p = 1\text{THz}$, $T = 300K$, $\mu_c = 0.2\text{eV}$, and $\tau = 2\text{ps}$. Figure 5a presents the variation in NPC under the different chemical potentials. The characteristic curves are observed to exhibit unphysical regions with increasing wave frequencies, and this is of no practical importance to the plasmonic industry. Furthermore, as chemical potential grows, the wave frequency band becomes narrow and characteristics curves shift toward the low-frequency region. Moreover, higher chemical potential leads to lower NPC as reported in [40, 41]. With increased chemical potential, graphene's valence and conduction bands become more distant from each other, resulting in the formation of an energy gap. In addition, this energy gap alters electron behavior, which impacts the propagation speed of wave-like disturbances, such as photons and electrons. The variation in NPC versus

frequency for different numbers of graphene layers is depicted in Fig. 5b. The cutoff frequency decreases with increasing layers of graphene. Furthermore, it is important to note that with an increasing number of graphene layers, the frequency band becomes narrow and characteristics curves are shifted towards lower NPC. Multilayer graphene exhibits this behavior due to the reduced mobility of carriers. Additionally, in graphene, electron and hole mobility decreases because of increased scattering and interactions with the lattice. Consequently, the wave's amplitude decreases, resulting in a decrease in the NPC. It is imperative to understand the NPC to tailor graphene's properties for various applications, including electronics, photonics, and nanophotonics. The variation in NPC for various plasma frequencies is depicted in Fig. 6a. As plasma frequency grows, NPC starts increasing and characteristics curves are shifted towards a high-frequency region as reported in [42]. Due to the increasing plasma frequency, the charged particles become more mobile and responsive to the EM waves. Consequently,
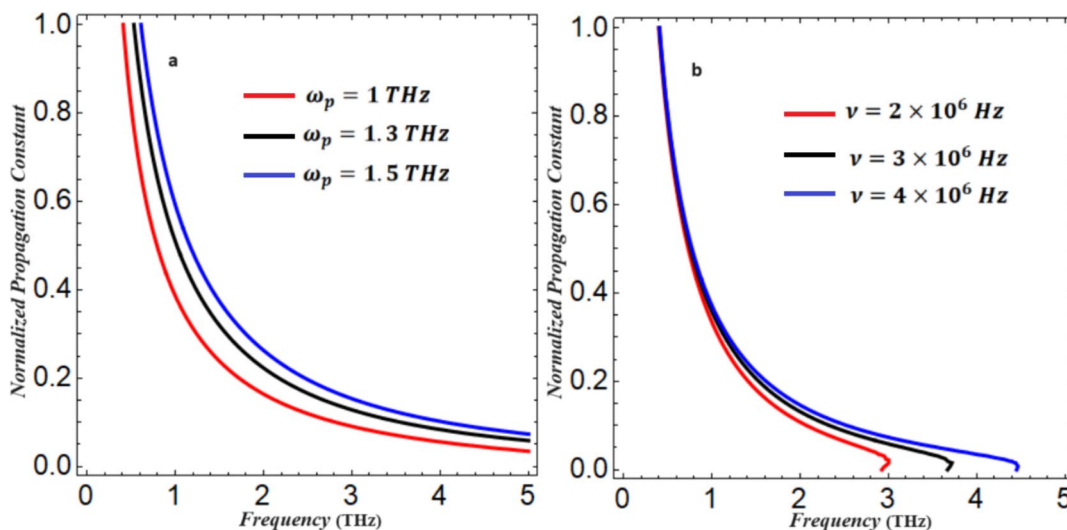

Fig. 6 Influence of the plasma frequency and collisional frequency on NPC for case II
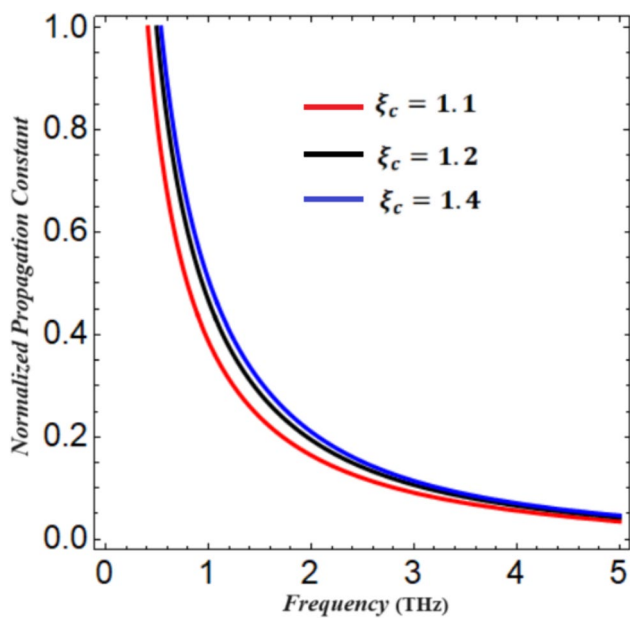
Fig. 7 Effect of the chemical potential and number of graphene layers on NPC for case II

the effective refractive index increases and the propagation constant increases as well. It is important to select the appropriate plasma frequency of an isotropic plasma to design and develop plasmonic devices. The variation in NPC for different collisional frequencies is analyzed in Fig. 6b. In this context, the EM wave frequency band increases from 0 to 5 THz and collisional frequency increases from $\upsilon = 2 \times 10^6$ Hz to $\upsilon = 4 \times 10^6$ Hz as indicated by red, black, and blue characteristic curves. It can be noted that the unphysical region vanished after the 1.2 THz frequency regime. In response to an increase in collisional frequency, both cutoff frequency and NPC increase. As the collisional frequency of an isotropic plasma increases, charged particles interact more intensely and frequently with each other. Furthermore, collisions between plasma particles occur more frequently, resulting in the exchange of energy and momentum. As a result of this transfer process, the wave's phase velocity is affected resulting in an increase in NPC. The influence of chirality versus EM wave frequency on the NPC is depicted in Fig. 7. Interestingly, higher chirality values are associated with higher NPCs and higher EM wave frequencies. Based on the results of the analysis above, the chirality parameter strongly depends upon the frequency of the EM waves. Furthermore, the EM wave frequency band starts squeezing for a higher chirality value. Additionally, NPC increases with the increase of the chirality parameter as reported in [33, 43, 44]. Consequently, NPC can be modulated by varying the chirality parameter.

Conclusion

The theoretical model was developed for a graphene-loaded waveguide structure surrounded by uniaxial chiral and plasma layers. For two types of uniaxial chiral medium, NPC parameters can be tuned by tuning graphene properties, including the chemical potential and the number of graphene layers, in addition to plasma properties, such as the plasma frequency, collisional frequency, and chirality parameters. It is concluded that case I support high frequency as compared to case II. The plasma frequency of isotropic plasma plays a crucial role in enabling the development of plasmonic-based devices. When plasma electrons oscillate at certain frequencies in resonance with the external electromagnetic field, their scattering properties are significantly enhanced. This resonance phenomenon can be exploited to design and fabricate plasmonic devices with various functionalities. The numerical results reflect that the presented study can be used to fabricate modulator plasmonic devices ranging from sensing and imaging to communication in the THz frequency regime.

Declarations

Ethical Approval Not applicable.

Competing Interests The authors declare no competing interests.

References

1. Huang, C.-P. and Y.-Y. Zhu, Plasmonics: manipulating light at the subwavelength scale. Active and Passive Electronic Components, 2007. 2007.

2. Gric T (2016) Surface-plasmon-polaritons at the interface of nano-structured metamaterials. Progress In Electromagnetics Research M 46:165–172

3. Gric T et al (2018) Tunable plasmonic properties and absorption enhancement in terahertz photoconductive antenna based on optimized plasmonic nanostructures. Journal of Infrared, Millimeter, and Terahertz Waves 39:1028–1038

4. Gric T, Hess O (2017) Controlling hybrid-polarization surface plasmon polaritons in dielectric-transparent conducting oxides metamaterials via their effective properties. J Appl Phys 122(19)

5. Gric T, Rafailov E (2022) Propagation of surface plasmon polaritons at the interface of metal-free metamaterial with anisotropic semiconductor inclusions. Optik 254:168678

6. Ioannidis T, Gric T, Rafailov E (2020) Surface plasmon polariton waves propagation at the boundary of graphene based metamaterial and corrugated metal in THz range. Opt Quant Electron 52:1–12

7. Novotny L, Hecht B (2012) Principles of nano-optics. Cambridge University Press

8. Ebbesen TW, Genet C, Bozhevolnyi SI (2008) Surface-plasmon circuitry. Phys Today 61(5):44–50

9. Homola J, Piliarik M (2006) Surface plasmon resonance (SPR) sensors. Springer

10. Ogawa S, Fukushima S, Shimatani M (2020) Graphene plasmonics in sensor applications: a review. Sensors 20(12):3563

11. Romagnoli M et al (2018) Graphene-based integrated photonics for next-generation datacom and telecom. Nat Rev Mater 3(10):392–414

12. Umair M et al (2023) Plasmonic characteristics of monolayer graphene in anisotropic plasma dielectric. Plasmonics 1–7

13. Edee K et al (2019) Coupling between subwavelength nano-slit lattice modes and metal-insulator-graphene cavity modes: a semi-analytical model. OSA Continuum 2(4):1296–1309

14. Rhouma MB (2021) Modeling and simulation of composite plasmonic structures based on graphene and metals. Université Clermont Auvergne

15. Rhouma MB, Meherzi O, Guizal B (2017) Strong coupling between a plasmonic waveguide and graphene surface plasmons. JOSA B 34(4):884–890

16. Rhouma MB, Oueslati M, Guizal B (2016) Surface plasmons on a doped graphene sheet with periodically modulated conductivity. Superlattices Microstruct 96:212–219

17. Rodrigo D et al (2015) Mid-infrared plasmonic biosensing with graphene. Science 349(6244):165–168

18. Wang J et al (2019) Theoretical design of mid-infrared graphene optical gas sensor based on slot Si core fiber. IEEE Photonics Technol Lett 31(13):1096–1099

19. Baqir M, Choudhury P (2013) Propagation through uniaxial anisotropic chiral waveguide under DB-boundary conditions. Journal of Electromagnetic Waves and Applications 27(6):783–793

20. Dong J-F, Li J (2012) Guided modes in the circular waveguide filled with uniaxial chiral medium. Int J Appl Electromagnet Mech 40(4):283–292

21. Ghaffar A, Alkanhal MA (2015) Electromagnetic reflection and transmission from a planar isotropic chiral-uniaxial chiral interface with optical axis normal to interface. Int J Appl Electromagnet Mech 47(3):805–817

22. Naheed M, Faryad M (2020) Excitation of surface plasmon–polariton waves in the prism-coupled configurations guided by reciprocal, uniaxially chiral, bianisotropic material. Optics Communications 465:125611

23. Gershman V, Ginzburg VL, Denisov N (1962) Propagation of electromagnetic waves in a plasma (ionosphere). US Atomic Energy Commission, Technical Information Service Extension

24. Kamp L, Weenink M (1983) Propagation of electromagnetic waves in a planarly stratified, isotropic, warm plasma with a resonance layer. Physica B+ C 122(1):89–112

25. Lee JH, Kalluri DK, Nigg GC (2000) FDTD simulation of electromagnetic wave transformation in a dynamic magnetized plasma. Int J Infrared Millimeter Waves 21:1223–1253

26. Shafranov V (1967) Electromagnetic waves in a plasma. Reviews of Plasma Physics: 3:1–157

27. Umair M et al (2024) Dyakonov waves generation at uniaxial chiral-plasma interface. Opt Express 32(3):4376–4386

28. Ghaffar A, Alkanhal MA (2015) Electromagnetic waves in uniaxial anisotropic chiral waveguides in magnetized plasma. Waves in Random and Complex Media 25(3):323–333

29. Umair M et al (2020) Transverse electric surface waves in ferrite medium surrounded by plasma layers. Journal of the European Optical Society-Rapid Publications 16(1):1–6

30. Umair M et al (2021) Dispersion characteristics of hybrid surface waves at chiral-plasma interface. Journal of Electromagnetic Waves and Applications 35(2):150–162

31. Azam M et al (2021) Dispersion characteristics of surface plasmon polaritons (SPPs) in graphene–chiral–graphene waveguide. Waves in Random and Complex Media 1–12

32. Gric T (2019) Tunable terahertz structure based on graphene hyperbolic metamaterials. Opt Quant Electron 51(6):202

33. Umair M et al (2023) Hybrid plasmon modes at chiroferrite-graphene interface. Plasmonics 1–7

34. Yaqoob MZ et al (2019) Characteristics of light–plasmon coupling on chiral–graphene interface. JOSA B 36(1):90–95

35. Saeed M et al (2021) Characteristics of hybrid surface plasmon polaritons at a chiral graphene metal interface in cylindrical waveguides. Opt Quant Electron 53:1–14

36. Saeed M et al (2021) Hybrid energy surface plasmon modes supported by graphene-coated circular chirowaveguide. Opt Mater 114:110869

37. Saeed M et al (2022) Graphene-based plasmonic waveguides: a mini review. Plasmonics 17(3):901–911

38. Gric T, Hess O (2017) Tunable surface waves at the interface separating different graphene-dielectric composite hyperbolic metamaterials. Opt Express 25(10):11466–11476

39. Umair M et al (2020) Characteristics of surface plasmon polaritons in magnetized plasma film walled by two graphene layers. J Nanoelectron Optoelectron 15(5):574–579

40. Shahid MU et al (2023) Electromagnetic waves in graphene-coated partially filled chiroplasma cylindrical waveguide. Plasmonics 18(5):1979–1989

41. Gric T (2021) Surface plasmons in metamaterial heterostructures. Waves in Random and Complex Media 31(6):1246–1257

42. Ali R, Zamir B, Shah H (2018) Transverse electric surface waves in a plasma medium bounded by magnetic materials. Results in physics 8:243–248

43. Umair M et al (2023) Light plasmon coupling in planar chiroplasma–graphene waveguides. Plasmonics 18(3):1029–1035

44. Xu J-P (1996) Propagation characteristics of a circular waveguide filled with a chiroferrite medium. Int J Infrared Millimeter Waves 17:193–203

Authors and Affiliations

Mutasem Z. Bani-Fwaz[1] · R. Bousbih[2] · Raad A. Khamis[3] · Mohamed S. Soliman[4] · Majid S. Jabir[5] · Hasan Majdi[6] · Mohamed Shaban[7] · Essam Elsayed Assem[7] · Sameerah I. Al-Saeedi[8] · N. M. A. Hadia[9] · Laiba[10]

✉ Laiba
laiba222rana@gmail.com

Mutasem Z. Bani-Fwaz
mbanifawaz@kku.edu.sa

R. Bousbih
rbousbih@ut.edu.sa

Raad A. Khamis
Rakplasma@gmail.com

Mohamed S. Soliman
soliman@tu.edu.sa

Majid S. Jabir
100131@uotechnology.edu.iq

Hasan Majdi
dr.hasanshker@mustaqbalcollege.edu.iq

Mohamed Shaban
mssfadel@aucegypt.edu

Essam Elsayed Assem
e_assem_2000@iu.edu.sa

Sameerah I. Al-Saeedi
sialsaeedi@pnu.edu.sa

N. M. A. Hadia
nmhadia@ju.edu.sa

[1] Department of Chemistry, College of Science, King Khalid University, P.O. Box 9004, 61413 Abha, Saudi Arabia

[2] Department of Physics, Faculty of Science, University of Tabuk, 71491 Tabuk, Saudi Arabia

[3] College of Sciences, Uruk University, Baghdad, Iraq

[4] Department of Electrical Engineering, College of Engineering, Taif University, 21944 Taif, Saudi Arabia

[5] Department of Applied Sciences, University of Technology, Baghdad, Iraq

[6] Department of Chemical Engineering and Petroleum Industries, Al-Mustaqbal University College, Babylon 51001, Iraq

[7] Department of Physics, Faculty of Science, Islamic University of Madinah, 42351 Madinah, Saudi Arabia

[8] Department of Chemistry, College of Science, Princess Nourah Bint Abdulrahman University, P.O. Box 84428, 11671 Riyadh, Saudi Arabia

[9] Department of Physics, College of Science, Jouf University, Al-Jouf, 2014 Sakaka, Saudi Arabia

[10] Department of Mathematics, Government College University Faisalabad, Faisalabad, Pakistan